

# WMAP Constraints on Quintessence

T. Barreiro,<sup>\*</sup> M. C. Bento,<sup>†</sup> N. M. Santos,<sup>‡</sup> and A. A. Sen<sup>§</sup>

*Departamento de Física, Instituto Superior Técnico  
Av. Rovisco Pais 1, 1049-001 Lisboa, Portugal*

(Dated: September 20, 2018)

We use recent results from the Wilkinson Microwave Anisotropy Probe (WMAP) for the locations of peaks and troughs of the Cosmic Microwave Background (CMB) power spectrum, together with constraints from large-scale structure, to study a quintessence model in which the pure exponential potential is modified by a polynomial factor. We find that the model is compatible with all the recent data for a wide range of cosmological and potential parameters. Moreover, quintessence is favoured compared to  $\Lambda$ CDM for  $n_s \approx 1$  and relatively high values of the average fraction of dark energy before last scattering (“early quintessence”); for  $n_s < 1$ , quintessence and  $\Lambda$ CDM give similar results, except for high values of early quintessence, in which case  $\Lambda$ CDM is favoured.

PACS numbers: 98.80.Cq

## I. INTRODUCTION

Recent cosmological observations suggest that there is a dark energy component to the energy density of the universe, which should be added to the matter component so as to reach the critical density. Theorists have considered various possibilities for the nature of this dark energy, notably a cosmological constant and quintessence, a dynamical scalar field leading to a time-varying equation of state parameter,  $w_\phi \equiv p_\phi/\rho_\phi$ . These models most often involve a single field [1, 2, 3, 4, 5, 6, 7, 8, 9, 10] or, in some cases, two coupled scalar fields [11, 12, 13]. Other possibilities for the origin of dark energy include the generalized Chaplygin gas proposal [14] and cardassian models [15].

In order to unravel the nature of dark energy, it is crucial to use observations so as to be able to discriminate among different models. In particular, the existence of a dark energy component affects the structure of the CMB power spectrum, which is particularly sensitive to the amount of dark energy at different epochs in cosmology. For instance, the locations of peaks and troughs depend crucially on the amount of dark energy today and at last scattering as well as the dark energy time-averaged equation of state, which are model-dependent quantities [16]. Hence, one can use the high precision measurements recently obtained by the BOOMERanG [17], MAXIMA-1 [18], Archeops [19] and, in particular, WMAP [20] observations to constrain dark energy models.

This study has already been performed for the case of a cosmological constant [21], the generalized Chaplygin gas

[22] and for some of the quintessence models that have been used in the literature, e.g. for the pure exponential potential [16, 23], a “leaping kinetic term” model [16, 24], Ratra-Peebles potential [16, 24, 25], a class of SUGRA potentials [25] and cosine-type quintessence [26].

The goal of this paper is to study the effect of a dark energy component defined by the quintessence potential proposed in Ref. [27]

$$V(\phi) = \left[ A + (\phi - \phi_0)^2 \right] e^{-\lambda\phi}, \quad (1)$$

on the location of the first three peaks and the first trough of the CMB power spectrum (for a first study of CMB anisotropies for this model see Ref. [28]). We also analyze the consequences of cluster abundance constraints on  $\sigma_8$ , the *rms* mass fluctuation on scales of  $8 h^{-1}$  Mpc.

The M-theory motivated potential of Eq. (1) leads to a model with some interesting features, namely there are two types of attractor solutions giving rise to an accelerating universe today, corresponding to permanent or transient acceleration [29]. Transient vacuum acceleration is a particularly appealing scenario that would also solve the apparent incompatibility between an eternally accelerating universe and string theory, at least in its present formulation, given that string asymptotic states are inconsistent with spacetimes that exhibit event horizons [30].

For both types of solutions, there is scaling of the densities early in the expansion history, with  $w_\phi = 1/3$ ,  $\Omega_\phi \approx 4/\lambda^2$  in the radiation dominated era and  $w_\phi = 0$ ,  $\Omega_\phi \approx 3/\lambda^2$  in the matter dominated epoch, followed by vacuum domination and accelerated expansion. Transient vacuum dominated solutions arise for  $A\lambda^2 > 1$ , in which case the potential has no local minimum or, for  $A\lambda^2 < 1$ , if the field  $\phi$  arrives at the local minimum with enough kinetic energy to roll over the potential barrier and continue rolling down the potential. Permanent vacuum domination occurs for  $A\lambda^2 < 1$ , if  $\phi$  gets trapped in the local potential minimum.

Our study of the dependence of the first three peaks and first trough locations on the potential parameters

<sup>\*</sup>Also at CENTRA, Instituto Superior Técnico, Lisboa. Email address: tiago@glencoe.ist.utl.pt

<sup>†</sup>Also at CFIF, Instituto Superior Técnico, Lisboa. Email address: bento@sirius.ist.utl.pt

<sup>‡</sup>Also at CFIF, Instituto Superior Técnico, Lisboa. Email address: ncsantos@cif.ist.utl.pt

<sup>§</sup>Also at CENTRA, Instituto Superior Técnico, Lisboa. Email address: anjan@x9.ist.utl.pt

in the  $(\Omega_m, h, n_s)$  cosmological parameters space, in view of WMAP's results, reveals that, for  $n_s \approx 1$ , the quintessence model of Eq. (1) is favoured as compared to the  $\Lambda$ CDM model, provided  $\lambda$ , which determines the average fraction of dark energy before last scattering, satisfies  $\lambda \lesssim 15$ . For  $n_s < 1$  and  $\lambda \lesssim 15$ , we find the opposite *i.e.*  $\Lambda$ CDM is favoured as compared to quintessence. As  $\lambda$  increases,  $\lambda \gtrsim 18$ , the model's results become comparable to  $\Lambda$ CDM's, independently of  $n_s$ , as should be expected since the average fraction of dark energy before last scattering becomes negligible. Moreover, the model presents a non-negligible fraction of dark energy at last scattering and during structure formation, typical of early quintessence models, leading to suppressed clustering power on small length scales as suggested by WMAP/CMB/large scale structure combined data [31].

## II. LOCATIONS OF PEAKS AND TROUGHS

We consider a spatially-flat Friedmann-Robertson-Walker (FRW) Universe containing a perfect fluid with barotropic equation of state  $p_w = w\rho_w$ , where  $w$  is a constant ( $w = 1/3$  for radiation and  $w = 0$  for dust), together with a scalar (quintessence) field with potential given by Eq. (1). The evolution equations for a spatially-flat FRW model with Hubble parameter  $H \equiv \dot{a}/a$  are

$$\begin{aligned} \dot{H} &= -\frac{1}{2} \left( \frac{4}{3} \rho_r + \rho_m + \dot{\phi}^2 \right), \\ \dot{\rho}_r &= -4H\rho_r, \\ \dot{\rho}_m &= -3H\rho_m, \\ \ddot{\phi} &= -3H\dot{\phi} - \frac{\partial V}{\partial \phi}, \end{aligned} \quad (2)$$

subject to the Friedmann constraint

$$H^2 = \frac{1}{3} \left( \rho_r + \rho_m + \frac{1}{2} \dot{\phi}^2 + V \right), \quad (3)$$

We work in units where  $M_P \equiv (8\pi G)^{-1/2} = \hbar = c = 1$ .

The CMB peaks arise from acoustic oscillations of the primeval plasma just before the Universe becomes transparent. The angular momentum scale of the oscillations is set by the acoustic scale  $\ell_A$  which for a flat Universe is given by [32, 33]

$$\ell_A = \pi \frac{\tau_0 - \tau_{ls}}{\bar{c}_s \tau_{ls}}, \quad (4)$$

where and  $\tau = \int a^{-1} dt$  is the conformal time,  $\tau_0$  and  $\tau_{ls}$  being, respectively, the conformal time today and at last scattering;  $\bar{c}_s$  is the average sound speed before decoupling

$$\bar{c}_s \equiv \tau_{ls}^{-1} \int_0^{\tau_{ls}} c_s d\tau,$$

$$c_s^{-2} = 3 + \frac{9}{4} \frac{\rho_b(t)}{\rho_\gamma(t)}, \quad (5)$$

with  $\rho_b/\rho_\gamma$  the ratio of baryon to photon energy density.

In an idealised model of the primeval plasma, there is a simple relation between the location of the  $m$ -th peak and the acoustic scale, namely  $\ell_m \approx m\ell_A$ . However, the location of the peaks is slightly shifted by driving effects and this can be compensated by parameterising the location of the  $m$ -th peak,  $\ell_m$ , as in [34, 35]

$$\ell_{p_m} \equiv \ell_A (m - \varphi_m) \equiv \ell_A (m - \bar{\varphi} - \delta\varphi_m), \quad (6)$$

where  $\bar{\varphi} \equiv \varphi_1$  is the overall peak shift and  $\delta\varphi_m \equiv \varphi_m - \bar{\varphi}$  is the relative shift of the  $m$ -th peak relative to the first. Eq. (6) is correct also for the location of troughs if we set, for instance,  $m = 3/2$  for the first trough and  $m = 5/2$  for the second trough. Although is not in general possible to derive analytically a relationship between the cosmological parameters and the peak shifts, one can use fitting formulae that describe their dependence on these parameters. Doran and Lilley [35] give accurate analytic approximations for the first three peaks and first trough, which can be found in the Appendix for convenience. Notice that, as the authors of Ref. [35] point out, although these formulae were obtained using a standard exponential potential, one expects the results to be fairly independent of the form of the potential (since the shifts are almost independent of post recombination physics) unless it is qualitatively very different from the exponential potential before last scattering.

The locations of the first two acoustic peaks and the first trough, from the WMAP measurements of the CMB temperature angular power spectrum are [20]

$$\begin{aligned} \ell_{p_1} &= 220.1 \pm 0.8, \\ \ell_{p_2} &= 546 \pm 10, \\ \ell_{d_1} &= 411.7 \pm 3.5; \end{aligned} \quad (7)$$

notice that all uncertainties are  $1\sigma$  and include calibration and beam errors. The location of the third peak is given by BOOMERanG measurements [36]

$$\ell_{p_3} = 825_{-13}^{+10}. \quad (8)$$

We have studied the location of the first three peaks and first trough in the  $(\Omega_m, h, n_s)$  cosmological parameter space for the potential Eq. (1), for different values of  $A$  and  $\lambda$ , slicing through the  $(\Omega_m, h)$  an  $(\Omega_m, n_s)$  planes. For each value of  $\lambda$  and  $A$ ,  $\phi_0$  is chosen such that  $\Omega_{tot} = 1$ . Given the rather strict bound  $\Omega_b h^2 = 0.0224 \pm 0.0009$  [20], we assume hereafter  $\Omega_b h^2 = 0.0224$ .

Our analysis in the  $(\Omega_m, h)$  plane shows that, for  $n_s = 1$ , the strongest constraints arise from the positions of the first and second peaks and, for clarity, we plot only the  $\ell_{p_1}, \ell_{p_2}$  contours corresponding to the WMAP bounds on

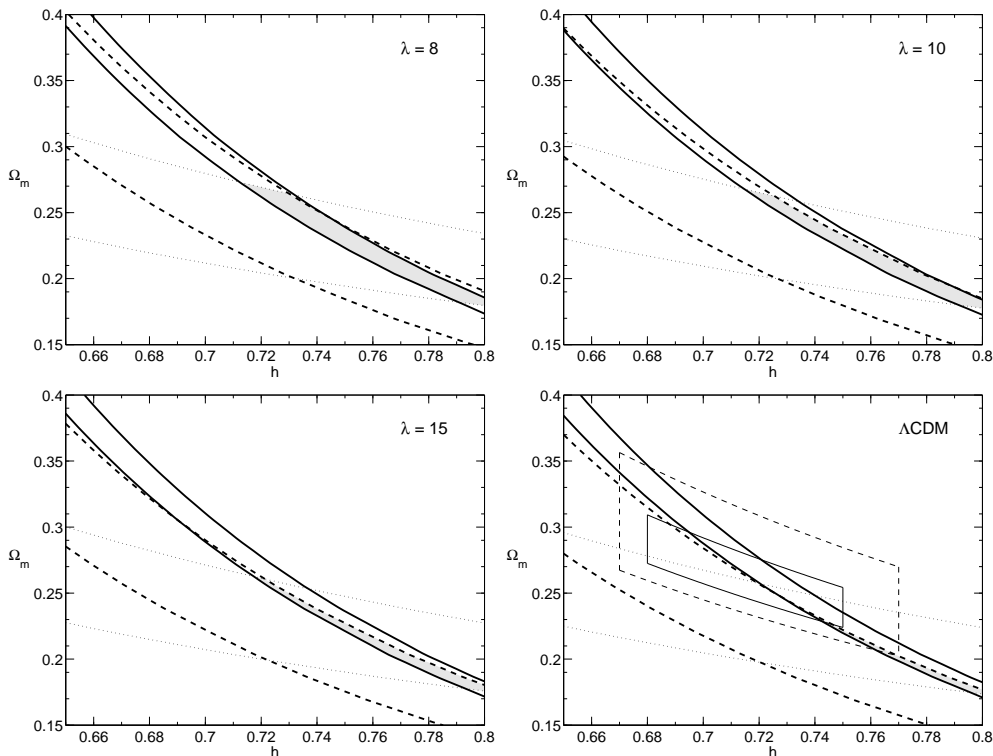


FIG. 1: Contour plots of the first and second Doppler peaks location in the  $(\Omega_m, h)$  plane for the potential Eq. (1), with  $A=0.0025$ , for different values of  $\lambda$  and spectral index  $n_s = 1$ . Full and dashed contours correspond to WMAP's bounds on, respectively,  $\ell_{p_1}$  and  $\ell_{p_2}$ , see Eq. (7). The dotted contours correspond to  $\sigma_8$  constraints. The intersection of all curves leads to the shaded allowed regions. We also show the corresponding contours for the  $\Lambda$ CDM model with  $n_s = 1$ ; the full and dashed boxes indicate, bounds from WMAP only and a combination of WMAP and other experiments on  $h$  and  $\Omega_m h^2$ , Eqs. (9) and (10) respectively.

these quantities, Eq. (7), for different values of  $\lambda$  and  $A = 0.0025$  (see Fig. 1); also shown are the  $\ell_{p_1}, \ell_{p_2}$  contours corresponding to the  $\Lambda$ CDM model for the same values of the cosmological parameters, where the dashed box represents WMAP's bounds on  $h$  and  $\Omega_m h^2$ , namely [20]

$$\Omega_m h^2 = 0.14 \pm 0.02, \quad h = 0.72 \pm 0.05 \quad (9)$$

The full box corresponds to the bounds obtained on these quantities from a combination of WMAP data with other CMB experiments (ACBAR and CBI), 2dFGRS measurements and Lyman  $\alpha$  forest data [20]

$$\Omega_m h^2 = 0.135^{+0.008}_{-0.009}, \quad h = 0.71^{+0.04}_{-0.03}. \quad (10)$$

For  $n_s = 0.95$ , the strongest constraints come from WMAP's bounds on  $\ell_{p_1}, \ell_{p_2}$  and  $\ell_{d_1}$ , see Fig. 2.

Finally, the results of our analysis in the  $(\Omega_m, n_s)$  plane, with  $h = 0.71$ , are shown in Fig. 3, where we plot the same contours as for Fig. 2.

### III. CONSTRAINTS FROM $\sigma_8$

We have also studied constraints resulting from  $\sigma_8$ , the *rms* density fluctuations averaged over  $8h^{-1}$ Mpc spheres.

Ref. [37] gives an estimate of the CMB-normalized  $\sigma_8$ -value for a very general class of quintessence models from  $\Omega_\phi(a)$ ,  $w_\phi(a)$  and the  $\sigma_8$ -value of the  $\Lambda$ CDM model with the same amount of dark energy today  $\Omega_\Lambda^0 = \Omega_\phi^0(\Lambda)$ :

$$\frac{\sigma_8^\phi}{\sigma_8^\Lambda} \approx (a_{eq})^3 \bar{\Omega}_\phi^{sf/5} (1 - \Omega_\Lambda^0)^{-(1+\bar{w}^{-1})/5} \sqrt{\frac{\tau_0^\phi}{\tau_0^\Lambda}}. \quad (11)$$

where  $a_{eq}$  is the scale factor at matter-radiation equality,  $\bar{\Omega}_\phi^{sf}$  is an average value for the fraction of dark energy during structure formation *i.e.* during the matter dominated era, before  $\Omega_\phi$  starts growing rapidly at scale factor  $a_{tr}$

$$\bar{\Omega}_\phi^{sf} \equiv [\ln a_{tr} - \ln a_{eq}]^{-1} \int_{\ln a_{eq}}^{\ln a_{tr}} \Omega_\phi(a) d \ln a. \quad (12)$$

The effective equation of state  $\bar{w}$  is an average value for  $w_\phi$  during the time in which  $\Omega_\phi$  is growing rapidly:

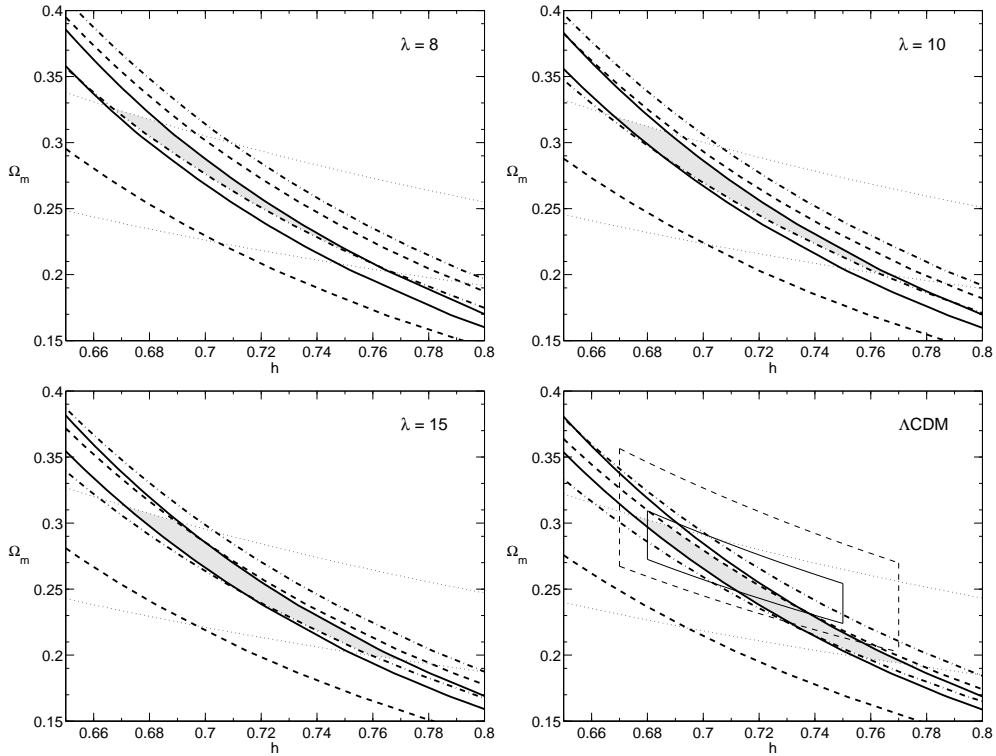


FIG. 2: As for Fig. 1 but with  $n_s = 0.95$  and the contours corresponding to the observational bounds on the first trough, Eq. (7), are also shown (dot-dashed contours).

$$\bar{w}^{-1} = \frac{\int_{\ln a_{\text{tr}}}^0 \Omega_\phi(a) w^{-1}(a) d \ln a}{\int_{\ln a_{\text{tr}}}^0 \Omega_\phi(a) d \ln a}. \quad (13)$$

In order to compute  $\sigma_8$  for the  $\Lambda$ CDM model, we use the definition

$$\sigma_8^2 \equiv \int_0^\infty \frac{dk}{k} \Delta^2(k) \left( \frac{3j_1(kr)}{kr} \right)^2, \quad (14)$$

with  $r = 8 h^{-1}$  Mpc and

$$\Delta^2(k) = \delta_H^2 \left( \frac{k}{H_0} \right)^{3+n} T^2(k), \quad (15)$$

where  $T(k)$  is the transfer function describing the processing of the initial fluctuations, for which we use the fitting function [38]

$$T(q) = \frac{\ln(1+2.34q)}{2.34q} \times \left[ 1 + 3.89q + (16.1q)^2 + (5.46q)^3 + (6.71q)^4 \right]^{-1/4}, \quad (16)$$

with [39]

$$q = \frac{k}{h\Gamma} \text{Mpc}, \quad \Gamma = \Omega_m h \exp \left[ -\Omega_b \left( 1 + \frac{\sqrt{2h}}{\Omega_m} \right) \right] \quad (17)$$

and  $\delta_H$  is the density perturbation at horizon crossing. A fit to the four-year COBE data gives [40]

$$10^5 \delta_H = 1.94 \Omega_m^{-0.785 - 0.05 \ln \Omega_m} \exp[a\tilde{n} + b\tilde{n}^2] \quad (18)$$

where  $\tilde{n} = n_s - 1$ ,  $a = -0.95$  and  $b = -0.169$  (assuming there are no gravitational waves). Taking into account reionization effects, Eq. (18) should be corrected; we use the fitting formula of Ref. [41]

$$\frac{\delta_H(\tau)}{\delta_H(\tau=0)} = 1 + 0.76\tau - 1.96\tau^2 + 1.46\tau^3, \quad (19)$$

where  $\tau$  is the optical depth. This formula is reliable up to  $\tau \approx 0.5$ ; we use  $\tau = 0.11$ , which is within the range of WMAP's bound,  $\tau = 0.166_{-0.071}^{+0.076}$  [20].

We compare our results for  $\sigma_8$  with large scale structure data. The recent study of the mass function of 300 clusters at redshifts  $0.1 < z < 0.2$  using early SDSS data yields  $\sigma_8 \Omega_m^{0.6} = 0.33 \pm 0.03$  [42].

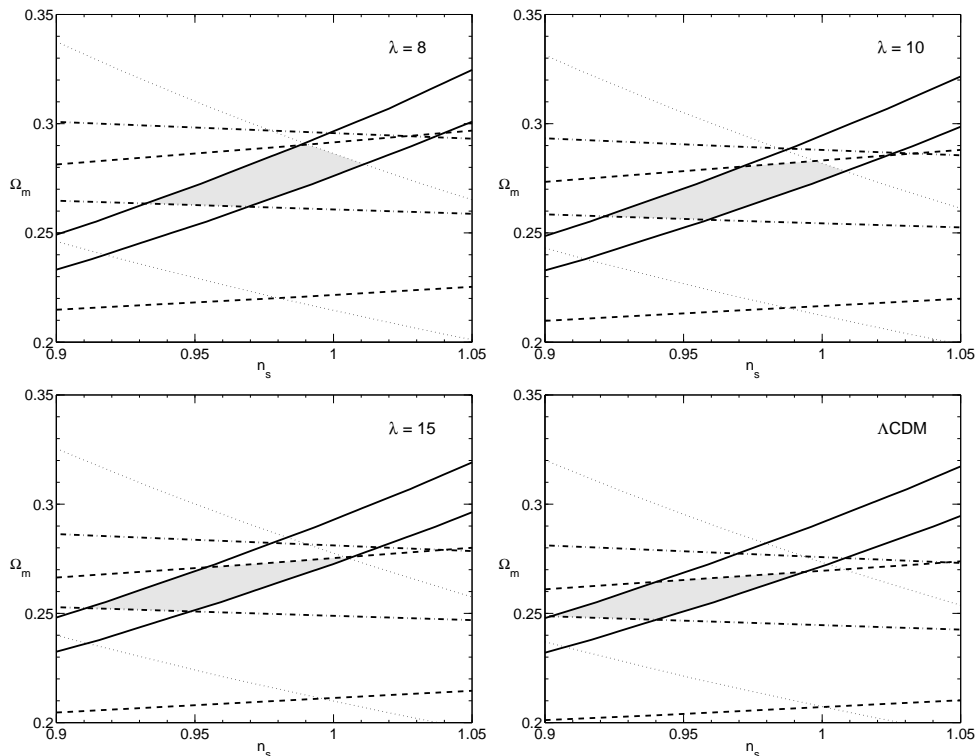


FIG. 3: Contour plots of the locations of the first and second peaks and first trough in the  $(\Omega_m, n_s)$  plane for the potential Eq. (1), with  $A=0.0025$ , for different values of  $\lambda$  and  $h = 0.71$ . Full, dashed and dot-dashed contours correspond to WMAP’s bounds on  $\ell_{p1}$ ,  $\ell_{p2}$  and  $\ell_{d1}$ , Eq. (7), respectively. The dotted contours correspond to  $\sigma_8$  constraints. We also show the equivalent plot for the  $\Lambda$ CDM model with  $h = 0.71$ .

Other cluster analysis (using eg. BCS, REFLEX and ROSAT data) yield different values:  $\sigma_8 = 0.43\Omega_m^{-0.38}$  [43],  $\sigma_8 = (0.508 \pm 0.019)\Omega_m^{-(0.253 \pm 0.024)}$  [44],  $\sigma_8 = (0.7 \pm 0.06)(\Omega_m/0.35)^{-0.44}(\Gamma/0.2)^{0.08}$  [45] and  $\sigma_8 = 0.38\Omega_m^{-0.48+0.27\Omega_m}$  [46].

The results of our study of  $\sigma_8$  constraints for the model of Eq. (1) are shown in Figs. 1 – 3 (dotted curves), where we have plotted the largest  $\sigma_8$  contours that are compatible both with the large scale structure fits mentioned above and the CMB computation, Eqs. (11) – (19).

#### IV. DISCUSSION AND CONCLUSIONS

Fig. 1 shows that, as  $\lambda$  increases, the allowed region becomes smaller and more similar to the  $\Lambda$ CDM model results; in particular, for  $\lambda = 15$ , the allowed region is only marginally larger than the one for  $\Lambda$ CDM model, which is quite small.

Notice that a lower bound on  $\lambda$  already exists from standard Big Bang Nucleosynthesis (BBN) and the observed abundances of primordial nuclides, which implies  $\Omega_\phi(\text{MeV}) < 0.045$ , or, considering a possible underestimation of systematic errors, the more conservative result  $\Omega_\phi(\text{MeV}) < 0.09$  [47]; these bounds require, respectively,  $\lambda > 9$  and  $\lambda > 6.5$ , for the model we are considering.

For  $n_s = 0.95$ , Fig. 2 shows that the allowed region becomes larger until  $\lambda \sim 15$  but does not change significantly for  $10 \lesssim \lambda \lesssim 18$ . Again, we find that, as  $\lambda$  increases,  $\lambda \gtrsim 18$ , the model’s results become more similar to the ones for the  $\Lambda$ CDM model.

Regarding the results of our analysis in the  $(\Omega_m, n_s)$  plane, with  $h = 0.71$ , Fig. 3, we see that the allowed region becomes smaller and shifts towards smaller values of  $n_s$  and  $\Omega_m$  as  $\lambda$  increases, in which case there is again a similarity with the  $\Lambda$ CDM model results.

We have also studied the dependence of the first three peaks and first trough locations on parameter  $A$ . We find that this dependence is extremely small and can safely be neglected. We notice that the values of  $A$  and  $\lambda$  we have previously considered all correspond to the permanent acceleration regime; however, as should be expected, changing  $A$  so as to reach the transient acceleration regime does not alter the analysis since this regime is not significantly different from the one where acceleration is permanent until the present, and therefore peak positions should not be affected.

Hence, the model’s behaviour depends essentially on parameter  $\lambda$ , which measures the amount of “early quintessence” (using the terminology of Ref. [31]) since  $\Omega_\phi^{ls} \sim 3/\lambda^2$ , where  $\Omega_\phi^{ls}$  is the average fraction of dark energy before last scattering

$$\bar{\Omega}_\phi^{ls} = \tau_{ls}^{-1} \int_0^{\tau_{ls}} \Omega_\phi(\tau) d\tau . \quad (20)$$

In fact, we obtain, for  $\lambda = 8$ ,  $0.039 < \bar{\Omega}_\phi^{ls} < 0.043$ , for the cosmological parameter range we are considering.

We conclude that, for  $n_s \approx 1$ , the  $\Lambda$ CDM model becomes increasingly disfavoured compared with the quintessence model of Eq. (1) as the amount of early quintessence becomes higher ( $\lambda \lesssim 15$ ). For  $n_s < 1$ , the opposite is true *i.e.*  $\Lambda$ CDM is favoured as compared to quintessence if  $\lambda \lesssim 15$ . Notice that, as  $\lambda$  increases ( $\lambda \gtrsim 18$ ), independently of the value of  $n_s$ , the model's results become comparable to  $\Lambda$ CDM's, as should be expected since  $\bar{\Omega}_\phi^{ls}$  decreases. Moreover, we see that quintessence is distinguishable from  $\Lambda$ CDM only for  $h < 0.73$  and  $n_s \approx 1$ .

Finally, we would like to mention that the non-negligible values we obtain for  $\bar{\Omega}_\phi^{sf}$  (e.g. for  $\lambda = 8$ , we get  $0.022 < \bar{\Omega}_\phi^{sf} < 0.026$ ), typical of early quintessence models, will lead, as shown in Ref. [31], to suppressed clustering power on small length scales as suggested by WMAP/CMB/large scale structure combined data.

### Acknowledgments

The work of T. Barreiro is fully financed by the Fundação para a Ciência e a Tecnologia (FCT) grant PPD/3512/2000. M.C. Bento acknowledges the partial support of FCT under the grant POCTI/1999/FIS/36285. The work of A.A. Sen is fully financed by the same grant. N.M.C. Santos is supported by FCT grant SFRH/BD/4797/2001.

### APPENDIX

We have used the analytic approximations for the phase shifts found in Ref. [35], which we reproduce here for completeness. The overall phase shift is given by

$$\bar{\varphi} = (1.466 - 0.466n_s) [a_1 r_*^{a_2} + 0.291 \bar{\Omega}_\phi^{ls}] , \quad (A.1)$$

where

$$\begin{aligned} a_1 &= 0.286 + 0.626\omega_b \\ a_2 &= 0.1786 - 6.308\omega_b + 174.9\omega_b^2 - 1168\omega_b^3 \end{aligned} \quad (A.2)$$

with  $\omega_b = \Omega_b h^2$ , are fitting coefficients,  $\bar{\Omega}_\phi^{ls}$  is given by Eq. (20) and

$$r_* \equiv \rho_r(z_{ls}) / \rho_m(z_{ls}) \quad (A.3)$$

is the ratio of radiation to matter at decoupling. A convenient fitting formula for  $z_{ls}$  is [48]

$$z_{ls} = 1048[1 + 0.00124w_b^{-0.738}[1 + g_1 w_m^{g_2}] , \quad (A.4)$$

where

$$\begin{aligned} g_1 &= 0.0783w_b^{-0.238}[1 + 39.5w_b^{0.763}]^{-1} , \\ g_2 &= 0.56[1 + 21.1w_b^{1.81}]^{-1} . \end{aligned} \quad (A.5)$$

The relative shift of the first acoustic peak is zero,  $\delta\varphi_1 = 0$ , and the relative shifts of the second and third peaks are given by

$$\delta\varphi_2 = c_0 - c_1 r_* - c_2 r_*^{-c_3} + 0.05(n_s - 1) , \quad (A.6)$$

with

$$\begin{aligned} c_0 &= -0.1 + \left(0.213 - 0.123\bar{\Omega}_{ls}^\phi\right) \\ &\quad \times \exp\left\{-\left(52 - 63.6\bar{\Omega}_{ls}^\phi\right)\omega_b\right\} , \\ c_1 &= 0.015 + 0.063 \exp(-3500\omega_b^2) , \\ c_2 &= 6 \times 10^{-6} + 0.137(\omega_b - 0.07)^2 , \\ c_3 &= 0.8 + 2.3\bar{\Omega}_{ls}^\phi + \left(70 - 126\bar{\Omega}_{ls}^\phi\right)\omega_b , \end{aligned} \quad (A.7)$$

and

$$\delta\varphi_3 = 10 - d_1 r_*^{d_2} + 0.08(n_s - 1) , \quad (A.8)$$

with

$$\begin{aligned} d_1 &= 9.97 + \left(3.3 - 3\bar{\Omega}_{ls}^\phi\right)\omega_b , \\ d_2 &= 0.0016 - 0.0067\bar{\Omega}_{ls}^\phi + \left(0.196 - 0.22\bar{\Omega}_{ls}^\phi\right)\omega_b \\ &\quad + \left(2.25 + 2.77\bar{\Omega}_{ls}^\phi\right) \times 10^{-5}\omega_b^{-1} . \end{aligned} \quad (A.9)$$

The relative shift of the first trough is

$$\delta\varphi_{3/2} = b_0 + b_1 r_*^{1/3} \exp(b_2 r_*) + 0.158(n_s - 1) \quad (A.10)$$

with

$$\begin{aligned} b_0 &= -0.086 - 0.079\bar{\Omega}_\phi^{ls} - (2.22 - 18.1\bar{\Omega}_\phi^{ls})\omega_b \\ &\quad - (140 + 403\bar{\Omega}_\phi^{ls})\omega_b^2 , \\ b_1 &= 0.39 - 0.98\bar{\Omega}_\phi^{ls} - \left(18.1 - 29.2\bar{\Omega}_\phi^{ls}\right)\omega_b \\ &\quad + 440\omega_b^2 , \end{aligned} \quad (A.11)$$

$$b_2 = -0.57 - 3.8 \exp(-2365\omega_b^2) , \quad (A.12)$$

Notice that the deviation of the acoustic extrema locations calculated using the above formulae from the values obtained by CMBfast code is  $< 3\%$  for a sufficiently wide range of parameters.

- 
- [1] B. Ratra, P.J.E. Peebles, *Phys. Rev.* **D37** 3406 (1988); *Ap. J. Lett.* **325** 117 (1988).
- [2] C. Wetterich, *Nucl. Phys.* **B302** 668 (1988).
- [3] R.R. Caldwell, R. Dave, P.J. Steinhardt, *Phys. Rev. Lett.* **80**, 1582 (1998).
- [4] P.G. Ferreira, M. Joyce, *Phys. Rev.* **D58**,023503 (1998) .
- [5] I. Zlatev, L. Wang, P.J. Steinhardt, *Phys. Rev. Lett.* **82**, 986 (1999).
- [6] P. Binétruy, *Phys. Rev.* **D60**, 063502 (1999) .
- [7] J.E. Kim, *JHEP* 9905, 022 (1999).
- [8] T. Barreiro, E. J. Copeland, N. J. Nunes, *Phys. Rev. D* **61**, 127301 (2000).
- [9] M.C. Bento and O. Bertolami, *Gen. Relativity and Gravitation* **31**, 1461 (1999); M.C. Bento, O. Bertolami, P.T. Silva, *Phys. Lett.* **B498**, 62 (2001).
- [10] J.P. Uzan, *Phys. Rev.* **D59**, 123510 (1999); T. Chiba, *Phys. Rev.* **D60** 083508 (1999); L. Amendola, *Phys. Rev.* **D60**, 043501 (1999); O. Bertolami, P.J. Martins, *Phys. Rev.* **D61**, 064007 (2000); N. Banerjee, D. Pavón, *Phys. Rev.* **D63**, 043504 (2001) ; *Class. Quantum Gravity* **18** 593 (2001); A.A. Sen, S. Sen, S. Sethi, *Phys. Rev.* **D63**, 107501 (2001); A.A. Sen, S. Sen, *Mod. Phys. Lett.* **A16**, 1303 (2001).
- [11] Y. Fujii, *Phys. Rev.* **D61**, 023504 (2000).
- [12] A. Masiero, M. Pietroni and F. Rosati, *Phys. Rev.* **D61**, 023504 (2000) .
- [13] M.C. Bento, O. Bertolami, N. C. Santos, *Phys. Rev.* **D65**, 067301 (2002) .
- [14] A. Kamenshchik, U. Moschella, V. Pasquier, *Phys. Lett.* **511**, 265 (2001); M.C. Bento, O. Bertolami and A.A. Sen, *Phys. Rev.* **D66**, 043507 (2002); N. Bilić, G.B. Tupper, R.D. Viollier, *Phys. Lett.* **B535**, 17 (2002).
- [15] K. Freese, M. Lewis, *Phys. Lett.* **B540**,1 (2002); S. Sen, A.A. Sen, astro-ph/0211634.
- [16] M. Doran, M. Lilley, J. Schwindt, C. Wetterich, *Astroph. J.* **559**, 501 (2001).
- [17] P. de Bernardis *et al.*, *Nature* (London) **404**, 955 (2000); A.E. Lange *et al.*, *Phys. Rev.* **D63**, 042001 (2001); C.B. Netterfield *et al.*, *Astrophys. J.* **571**, 604 (2002).
- [18] S. Hanany *et al.*, *Astrophys. J.* **545**, L5 (2000); A. Balbi *et al.*, *Astrophys. J.* **545**, L1 (2000) [Erratum-*ibid.* **558**, L145 (2001)].
- [19] A. Benoît *et al.*, astro-ph/0210306.
- [20] D.N. Spergel *et al.*, astro-ph/0302209.
- [21] W. Hu, astro-ph/0210696.
- [22] M.C. Bento, O. Bertolami, A.A. Sen, astro-ph/0210468.
- [23] D. Di Domenico, C. Rubano, P. Scudellaro, astro-ph/0209357.
- [24] M. Doran, M. Lilley, C. Wetterich, *Phys. Lett.* **B528**, 175 (2002).
- [25] P. Brax, J. Martin, A. Riazuelo, *Phys. Rev.* **D62**, 103505 (2000).
- [26] M. Kawasaki, T. Moroi, T. Takahashi, *Phys. Rev. D* **64**, 083009 (2001).
- [27] A. Albrecht, C. Skordis, *Phys. Rev. Lett.* **84**, 2076 (2000).
- [28] A. Albrecht, C. Skordis, *Phys. Rev.* **D66**, 043523 (2002).
- [29] J. Barrow, R. Bean, J. Magueijo, *Mon. Not. Roy. Astron. Soc.* **316**, L41 (2000).
- [30] S. Hellerman, N. Kaloper, L. Susskind, *JHEP* **0106**, 003 (2001); W. Fischler, A. Kashani-Poor, R. McNess, S. Paban, *JHEP* **0107**, 003 (2001); E. Witten, hep-th/0106109.
- [31] R.R. Caldwell, M. Doran, C.M. Müller, G. Schäfer, C. Wetterich, astro-ph/0302505.
- [32] W. Hu, N. Sugiyama, *Astrophys. J.* **444**, 489 (1995).
- [33] W. Hu, N. Sugiyama, J. Silk, *Nature* **386**, 37 (1997).
- [34] W. Hu, M. Fukugita, M. Zaldarriaga, M. Tegmark, *Astrophys. J.* **549**, 669 (2001).
- [35] M. Doran, M. Lilley, *Mon. Not. Roy. Astron. Soc.* **330**, 965 (2002).
- [36] J.E. Ruhl *et al.*, astro-ph/0212229.
- [37] M. Doran, J. Schwindt, C. Wetterich, *Phys. Rev.* **D64**, 123520 (2001).
- [38] J.M. Bardeen, J.R. Bond, N. Kaiser, A.S. Szalay, *Astrophys. J.* **304**, 15 (1986).
- [39] N. Sugiyama, *Astrophys. J. Suppl.* **100**, 281 (1995).
- [40] E.F. Bunn, M. White, *Astrophys. J.* **480**, 6 (1997).
- [41] L.M. Griffiths, A Liddle, astro-ph/0101149.
- [42] N.A. Bahcall *et al.*, *Astrophys. J.* **585**, 182 (2003).
- [43] T.H. Reiprich and H. Böhringer, *Astrophys. J.* **567**, 716 (2002).
- [44] S.W. Allen, R.W. Schmidt, A.C. Fabian and H. Ebeling, *Mon. Not. Roy. Astron. Soc.* **334**, L11 (2002).
- [45] U. Seljak, 2002, *MNRAS* **337**, 769 (2002).
- [46] P.T.P. Viana, R.C. Nichol and A.R. Liddle, *Astrophys. J.* **569**, L75 (2002).
- [47] R. Bean, S. H. Hansen, A. Melchiorri, *Phys. Rev.* **D64**, 103508 (2001).
- [48] W. Hu, N. Sugiyama, *Astrophys. J.* **471**, 30 (1996).